JOURNAL OF APPLIED ELECTROCHEMISTRY 21 (1991) 255–260

Influence of some organic compounds on the corrosion mechanism of carbon steel (XC 38) in 3% NaCl I. dodecyl sodium phosphonate ($C_{10}H_{21}PO_3Na_2$) and n-undecylimidazole ($C_{14}H_{26}N_2$) surfactants

F. DABOSI

Equipe de Recherche Associée au CNRS no 263, Laboratoire de Métallurgie Physique, Ecole Nationale Supérieure de Chimie, 31077 Toulouse Cédex, France

Y. DERBALI

Department of Chemistry, Faculty of Sciences, Tunis, Tunisia

M. ETMAN

Laboratoire d' Electrochimie Interfaciale du CNRS, 1 Place A. Briand, 92195 Meudon Cédex, France

A. SRHIRI*

Université Mohamed V, Faculté des Sciences, Kenitra, Maroc

A. DE SAVIGNAC

Laboratoire IMRCP Université Paul Sabatier, 31062 Toulouse, France

Received 12 December 1989; revised 22 May 1990

The electrochemical behaviour of carbon steel (XC38) in stirred and aerated 3% NaCl solution has been investigated using a rotating disc electrode. Steady-state and transient measurements have been carried out. The influence of surfactant additives on the corrosion process is reported.

1. Introduction

From the literature it is clear that the electrochemical impedance measurements carried out at different points in the current-potential response allow identification of the elementary steps involved in corrosion and protective processes [1–4]. This technique has been applied to examine the influence of the addition of surfactants on the electrochemical behaviour of carbon steel (XC38) in aerated and stirred 3% NaCl. With surfactants added to the electrolyte some investigators have already shown that the presence of liophile and hydrophobe groups favours the adsorption process at the electrode surface [5–8]. Accordingly two principal results have to be noted: (i) the corrosion inhibition efficiency is maximized when the inhibitor concentration is near the critical micellar concentration (CMC); (ii) the maximal inhibitor efficiency is generally observed when the surfactant has a hydrophobic chain with 10 to 13 carbon atoms. Activity-structure correlations in relation to the physicochemical behaviour of the surfactants in solution (micellisation phenomenon) have been established.

In the present paper a study of the effect of two surfactants (dodecyl sodium phosphonate and n-undecylimidazole) on the corrosion mechanism of carbon steel (XC38) in 3% NaCl has been carried out. The hydrophobic chain was maintained constant while the nature of the liophilic group of the studied molecule was modified. The head groups concerned here are phosphonate and imidazole. In further work we studied the effect of the surfactant dodecyl sodium phosphate ($C_{10}H_{21}PO_4Na_2$) and the non-surfactant orthoaminothiophenol (C_6H_7NS); results and the general conclusions are submitted in the same issue [9].

2. Experimental details

The carbon steel (XC38)† used in the present study had elemental composition (other than Fe) as follows: $0.35 \leqslant C \leqslant 0.40$; $0.50 \leqslant Mn \leqslant 0.80$; $0.10 \leqslant Si \leqslant 0.40$; P and $S \leqslant 0.0035$.

For electrochemical measurements, a 300 ml volume three electrode cell was used. The reference electrode was always saturated calomel (SCE), the counter electrode was a large surface area cylindrical grid of platinum. The carbon steel working electrode had

* To whom all correspondence should be addressed.

† Terminology given by l'Association Française pour la Normalisation (AFNOR).

0021-891X/91 $03.00 + .12

a cross-section of 1 cm^2 and was covered with an impermeable heat shrunk film. It was bolted onto a rotation support. The electrode surface was polished with a silicon carbide emery cloth (grade 80), rinsed thoroughly with distilled water, ultrasonically cleaned and degreased with alcohol and finally dried with hot air. The corrosive medium was a 3% pure NaCl solution (pro-analysis grade) dissolved in double distilled water.

In this paper, as in a further work [9], studies were all carried out at room temperature except in the case of n-undecylimidazole. For this compound, a temperature of 30° C was used because the Kraft point of this compound is higher than that of the other compounds.

The surfactant organic compounds studied in this paper were: (i) n-undecylimidazole ($C_{14}H_{26}N_2$); and (ii) dodecyl sodium phosphonate ($C_{10}H_{21}PO_3Na_2$). Both surfactants were synthesized in the laboratory of molecular interaction and chemical-photochemical reactivity at the Paul Sabatier University, France.

Previous studies [10, 11] permitted the choice of the concentration, 5×10^{-2} M for the $C_{10}H_{21}PO_9Na_2$ and 10^{-2} M for the $C_{14}H_{26}N_2$. These are in both cases higher than the critical micellar concentration (CMC), 2.1×10^{-2} M for the first and 10^{-3} M for the second surfactant. It has also shown that the inhibition efficiency seems to be constant with concentrations higher than the CMC. [5–8].

The current–potential curves were recorded in either galvanostatic or potentiostatic modes. Electrochemical impedance measurements made over a frequency range 100 kHz down to a few mHz. The response was analysed using a Schlumberger-Solartron 1174. Description and details of the set-ups used have been published elsewhere [12, 13]. In the Niquist complex impedance $Z = R - jG$, where R is the real component, G is the imaginary component and $j = \sqrt{(-1)}$.

3. Results and discussion

3.1. *Carbon steel (XC38) – 3% NaCl + 5 × 10^{-2} M $C_{10}H_{21}PO_3Na_2$.*

In Fig. 1, the cathodic potentiostatic curves at the interface carbon steel (XC38) - 3% NaCl (a) without and (b) with dodecyl sodium phosphonate are shown. The same figure also shows the values of i_L calculated from the Levich equation [14]. The symbols i and I refer to current density and applied (or measured) current, respectively. Thus,

$$I_L = 0.62nFC_\infty D^{2/3} \nu^{-1/6} \omega^{1/2} A \qquad (1)$$

where n is the number of electrons exchanged during oxygen reduction ($O_2 + 2H_2O + 4e \longrightarrow 4OH^-$); F is the Faraday constant (~96 500 C), C_∞ is the dissolved oxygen concentration (2×10^{-7} mol cm^{-3} at 25° C); ν is the kinematic viscosity of the medium (10^{-2} cm^2 s^{-1} at 25° C); D is the diffusion coefficient of oxygen (2×10^{-5} cm^2 s^{-1}); ω ($= 2\pi N$; N is the number of electrode revolutions per unit time) is the angular rotational speed of the electrode (104.6 rad s^{-1}); and A is the working electrode area (1 cm^2). The current value calculated from Equation 1 is higher than the experimental value obtained with (XC38)–3%NaCl interface. The low experimental value of i_L has been attributed to the development of strongly adsorbed corrosion film products on the working electrode [4]. The corrosion products were produced with the electrode maintained at E_{corr}. This film acts as a barrier to the oxygen reduction reaction. Additionally, this reaction is totally diffusion controlled ($i_{corr} = i_L = 550\,\mu A\,cm^{-2}$ [3]). In the presence of 5×10^{-2} M dodecyl sodium phosphonate, the diffusion plateau is not clear. The value of the cathodic current density measured at −900 mV is less important than i_L obtained in the case of the blank. In this case, the working electrode surface is very probably free of corrosion products. Moreover, the addition of this surfactant shifts the corrosion potential towards more positive values. Consequently i_{corr} can be determined by the extrapolation of the cathodic Tafel line. The values of E_{corr}, b_c (slope of cathodic Tafel line) and i_{corr} ($25\,\mu A\,cm^{-2}$) explain the existence of a large potential domain with mixed kinetics. The inhibition efficiency can be calculated from:

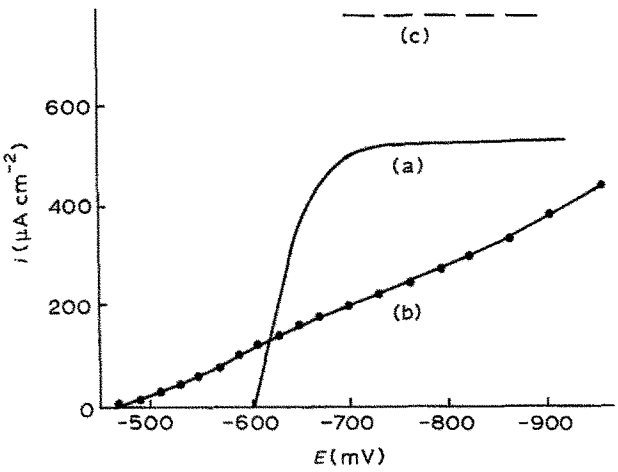

Fig. 1. Steady-state cathodic current-voltage relationship for a rotating disc electrode (N = 1000 r.p.m.). (a) Carbon steel (XC38)–3% NaCl, (b) carbon steel (XC38)–3% NaCl + 5×10^{-2} M $C_{10}H_{21}PO_3Na_2$ (c) Levich current. The electrode was maintained for 30 min at E_{corr} before measurements.

$$E(\%) = \frac{i_{corr} - i'_{corr}}{i_{corr}} \times 100 \qquad (2)$$

where i_{corr} and i'_{corr} are the corrosion current densities in the absence and in the presence of additives respectively. The inhibition efficiency was found to be 95%. Changes in the form of the response in the presence of the inhibitor can then be attributed to changes in the process at the inhibitor-metal/solution interface.

Figure 2 shows a galvanostatic electrochemical impedance diagram in the complex plane. The experimental conditions were $i = 0\,\mu A\,cm^{-2}$ and N = 1000 r.p.m. The electrode was maintained for 2 h at its free corrosion potential, before the measurements were made: a capacity loop appears. It is important to

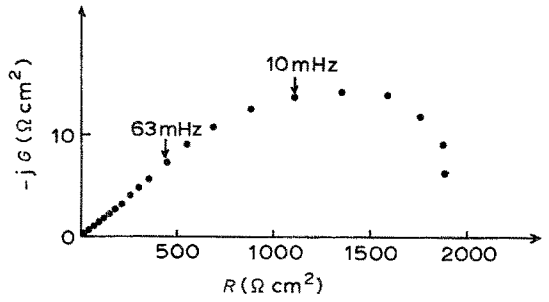

Fig. 2. Diagram of electrochemical galvanostatic impedance of the rotating disc electrode (N = 1000 r.p.m.). The electrode was maintained for 2 h at E_{corr} in 3% NaCl + 5 × 10^{-2} M $C_{10}H_{21}PO_3Na_2$ before measurements.

note that this loop is not closed at low frequencies (i.e. frequencies at which it is difficult to work due to the very large time required for measurements and the long term instability of the interfacial electrochemical system). However, the intersection with the real axis of the extrapolated part at zero frequency gives the value (R_p + R_E), where R_p is the polarization resistance and R_E is the resistance of the electrolyte. The calculated value (~2000 Ω cm²) is in a good agreement with the slope of the steady state current–voltage curve $(dE/di)_{i\longrightarrow 0}$ (see Fig. 1).

Using the same experimental conditions, the impedance diagrams were recorded in the absence of the inhibitor with the working electrode maintained for different periods at its free corrosion potential, E_{corr}, before the measurements were initiated (see Fig. 3). With a critical immersion time of 30 min, two loops appear and become better defined with increasing immersion time. In a recent, in-depth analysis [15] the low frequency loop (BF) has been identified with mass transport in both the liquid phase as well as through the surface film of corrosion products. This analysis prompted Dabosi and co-workers [15] to

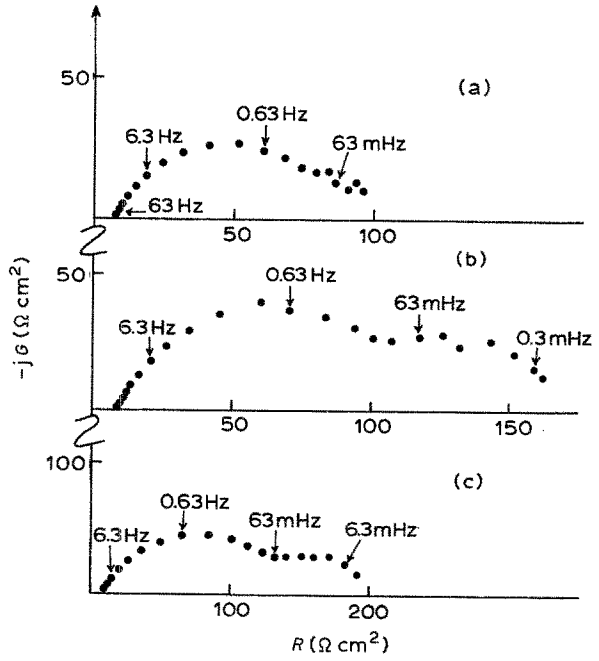

Fig. 3. Influence of pretreatment time of the interface carbon steel (XC38)–3% NaCl on the electrochemical impedance diagrams: (a) 30 min, (b) 2 h and (c) 5 h. Conditions: i = 0 μA cm^{-2} (E_{corr}); N = 1000 r.p.m.

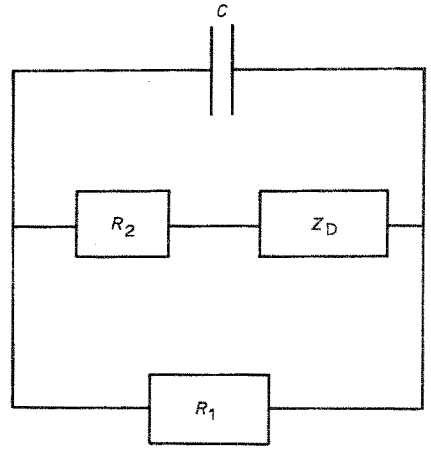

Fig. 4. Equivalent circuit of the carbon steel–3% NaCl interface [15]; R_1 and R_2 are respectively the anodic and cathodic resistances for charge transfer, Z_D is the diffusion impedance and C is the double layer capacity.

propose an equivalent circuit for the carbon steel–3% NaCl interface (see Fig. 4).

Values of the capacitance, C, calculated using the relation $C = (2\pi F_c R_p)^{-1}$, associated with the HF loops of Fig. 3, are high and also increase with immersion time. The highest value of these capacitances (~1.4 mF cm^{-2} ⟶ 2.2 mF cm^{-2}) has been attributed to the presence of the film of corrosion products which induces a considerable increase in the specific surface area [16]. The value of C determined in the presence of ethylenediamine under the same conditions was also found to be high, 500 μF cm^{-2}; this supports the hypothesis of the increase in the specific surface area.

The high inhibition efficiency of $C_{10}H_{21}PO_3Na_2$ (E = 95.5%) at the concentration used in these studies, suggests that the high value is due to the presence of the film of corrosion product. Consequently the diagram shown in Fig. 5 needs to be analysed in more detail.

The value of C from the data in Fig. 4, compared to the value associated with the high frequency (HF) loops in the absence of the inhibitor implies that the capacity loop only represents the charge transfer process. With this assumption, the polarization resistance R_p will be equal to the transfer resistance

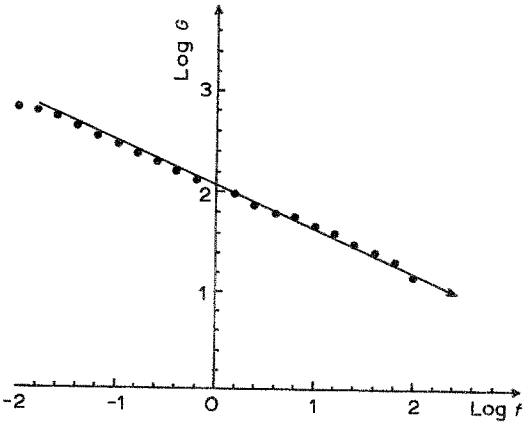

Fig. 5. Experimental confirmation of the existence of a Warburg impedance when 5 × 10^{-2} M dodecyl sodium phosphonate is added to the 3% NaCl electrolyte. G is the imaginary component of the impedance in the complex plane and f is the frequency.

R_T. Calculation of corrosion rate using the relation of Stern and Geary [17], gives a corrosion current, i_{corr}, of $14\,\mu A\,cm^{-2}$ instead of $25\,\mu A\,cm^{-2}$ obtained from the extrapolation of the Tafel line corrected for diffusion as follows:

$$1/i = 1/i^* + 1/i_L \quad (3)$$

where i is the measured current intensity, i^* is the intensity of corrected current and i_L is the limiting diffusion current. On the basis of the calculated value of the corrosion current, i_{corr}, assuming that $R_T \ll R_p$, the observed capacitive loop does not correspond to one time constant. This must indicate the simultaneous occurrence of charge transfer and mass transport.

A further analysis of the HF part of the diagram in Fig. 2 reveals a linear region of approximately unit slope. Such behaviour generally characterizes a Warburg impedance [18] and suggests a relaxation of concentration.

The slope of the linear relationship between values of the imaginary component of the impedance in the complex plane and frequencies (Fig. 5) was found to be -0.43. The theoretical slope for pure Warburg impedance would be -0.5, so it can be reasonably assumed that, within experimental error, the HF impedance corresponds to Warburg impedance. It is important to note that this phenomenon appears with both low and high rotating speeds ($N = 600$ and 2400 r.p.m.). The difference between the experimental and theoretical values of the slope is justified below.

The impedance diagram in Fig. 2 starts at high frequencies with a diffusion impedance and, as the frequency is reduced, no loop which could be associated with charge transfer appears. This can be explained if we consider the equivalent circuit in Fig. 4. It is important to note that the circuit takes into account the mixed nature of the corrosion potential. Consequently cathodic and anodic branches in parallel are presented. R_1 and R_2 are the anodic and cathodic charge transfer resistances respectively while Z_D is the classical diffusion impedance.

$$Z_D = R_D\left(\frac{\text{th}\,(j\omega'\delta^2/D)^{1/2}}{(j\omega'\delta^2/D)^{1/2}}\right) \quad (4)$$

where $\omega' = 2\pi f$; D is the diffusion coefficient; δ is the diffusion layer thickness; and 'th' is the hyperbolic tangent.

We have recently reported that if $R_1 \gg R_2$ and if R_1 and R_D are of the same order of magnitude, the simulated faradaic impedance, Z_F, shows, in the complex plane, close similarities with experimental values noticed in the present work [16]. The observed capacitative loop represents both the cathodic transport process as well as the anodic charge transfer process. It is not simply a charge transfer loop. Because of the finite values of R_1 in parallel with both R_2 and Z_D, the classical form of the diffusion impedance is not observed. This can also explain the difference between the experimental and the theoretical slope obtained from the representation $\log G = f(\log F)$ in Fig. 5. Figure 6 shows the electrochemical cathodic

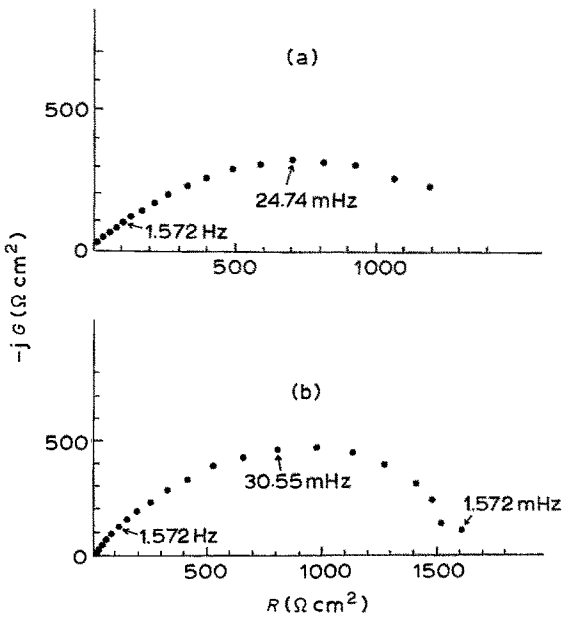

Fig. 6. Galvanostatic cathodic impedance diagrams of the interface carbon steel (XC38)–3% NaCl + 5×10^{-2} M dodecyl sodium phosphonate for two different current densities. (a) $i_c = 160\,\mu A\,cm^{-2}$, (b) $i_c = 80\,\mu A\,cm^{-2}$. Pretreatment time = 45 min and $N = 1000$ r.p.m.

impedance diagrams obtained at two different applied current densities for the interface carbon steel–3% NaCl + 5×10^{-2} M dodecyl sodium phosphonate: (a) $i_c = 160\,\mu A\,cm^{-2}$, (b) $80\,\mu A\,cm^{-2}$.

In the anodic range (Fig. 7), the diagrams are characterized by only one capacity loop. Because of difficulties in obtaining well defined steady-state conditions a dispersion phenomenon was observed in the low frequency (BF) domain, particularly for maximum current densities at which it is difficult to work below 1 Hz.

Estimated values of resistance R, characteristic frequency, F_c, and of the associated capacity to the capacity loop, C, are reported in Table 1.

It should be noted that for low anodic overvoltages ($i_\alpha = 20$ and $50\,\mu A\,cm^{-2}$) at which the cathodic reaction is still active, capacity values were found to be one order of magnitude higher than the value of C recorded at the corrosion potential ($i = 0\,\mu A\,cm^{-2}$). Those high values were previously justified by the fact

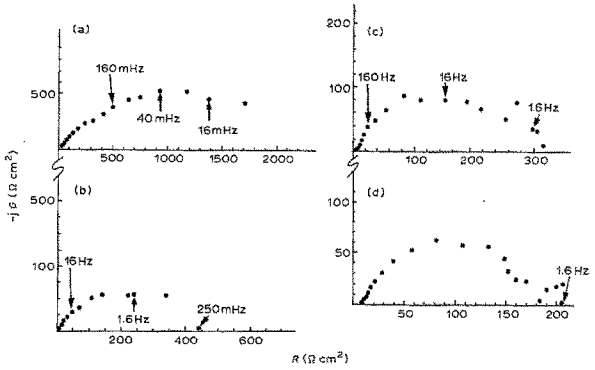

Fig. 7. Electrochemical anodic galvanostatic impedance diagrams at different current densities. (a) $i_\alpha = 20\,\mu A\,cm^{-2}$, (b)$i_\alpha = 500\,\mu A\,cm^{-2}$, (c) $i_\alpha = 1\,mA\,cm^{-2}$, (d) $I_\alpha = 2\,MA\,cm^{-2}$. In all cases $N = 1000$ r.p.m. and the electrode was maintained for 1 h at E_{corr} before measurements.

Table 1. R, F and C values from galvanostatic anodic impedance diagrams of carbon steel electrode in 3% NaCl + 5 × 10^{-2} M $C_{10}H_{21}PO_3Na_2$; N = 1000 r.p.m.

i_a ($\mu A\ cm^2$)	20	50	120	200	500	1000	2000
$R(\Omega\,cm^2)$	1800	1500	1400	750	440	350	170
f(Hz)	0.040	0.055	0.160	0.530	2.500	16.000	250.000
$C(\mu F\,cm^{-2})$	2210	1930	710	400	145	28	4

that the capacitive loop represents both the anodic charge transfer and the cathodic mass transport processes.

Starting at 120 $\mu A\,cm^{-2}$, the capacity decreases considerably and regularly with the overvoltage to reach a very low value ($\sim 4\,\mu F\,cm^{-2}$) at i_α = 2 mA Cm^{-2}. From the above observations, the formation of a superficial thick film is suggested. These observations indicate that there is a direct relationship between the compactness of the film and the initial dissolution rate corresponding to the applied current density. The origin of this thick film may be due to a transformation of the initial and relatively porous film which results from the initial metal dissolution process.

The observed capacitive loop then represents both the film and charge transfer effect, the low capacity value resulting from the joined effects of a blocked surface and an additive with a hydrophobic head group [10].

3.2. *Carbon steel (XC38) – 3% NaCl + 10^{-2} M $C_{14}H_{26}N_2$*

The potentiostatic cathodic response with 10^{-2} M $C_{14}H_{26}N_2$ at a rotating speed N = 1000 r.p.m. after the electrode had been maintained for 30 min at its free E_{corr} before measurements were initiated, is given in Fig. 8. This indicates that the addition of n-undecylimidazole ($C_{14}H_{26}N_2$) shifts the corrosion potential considerably towards positive values. A limiting current plateau appears and the density of the corresponding current is much higher than in the blank solution, but this is still lower than the corresponding theoretical value for a uniformly reactive surface.

A mixed kinetic domain can also be demonstrated with a cathodic Tafel line of slope 188 ± 10 mV decade^{-1}. The extrapolation of this linear relation to the corrosion potential gives a value of i_{corr} = 40 $\mu A\,cm^{-2}$. The corresponding inhibition efficiency was found to be 93%.

For the cathodic region, the results are shown in Fig. 9. Comparison with the blank results indicates that the presence of $C_{14}H_{26}N_2$ increases the overvoltage in the vicinity of E_{corr} and that the form obtained does not seem to be influenced by high overvoltages. The extrapolation of the anodic Tafel relationship (slope of 178 mV (decade))$^{-1}$ to E_{corr} gave i_{corr} as 35 $\mu A\,cm^{-2}$.

The corrosion rate calculated from iron concentration determined by atomic absorption was estimated to be $\sim 50\,\mu A\,cm^{-2}$. According to the above results, $C_{14}H_{26}N_2$ acts as a corrosion inhibitor and modifies the mechanisms of the electrochemical anodic and cathodic processes. With the impedance technique the inhibition characteristics are clearly shown.

The electrochemical impedance diagrams in Fig. 10 are characterized by a capacitive loop with dispersion at low frequencies (BF). The results shown are independent of electrode rotation speed. In the anodic region, the product $R\ i_\alpha$ is constant where R is the diameter of the capacitive loop and i_α is the applied anodic current density (see Table 2). The value of 2.3 R i_α, representing the anodic Tafel slope, is 161 ± 10 mV. This value is close to that observed in the steady-state anodic measurements (178 ± 15 mV), but is much higher than that found in the

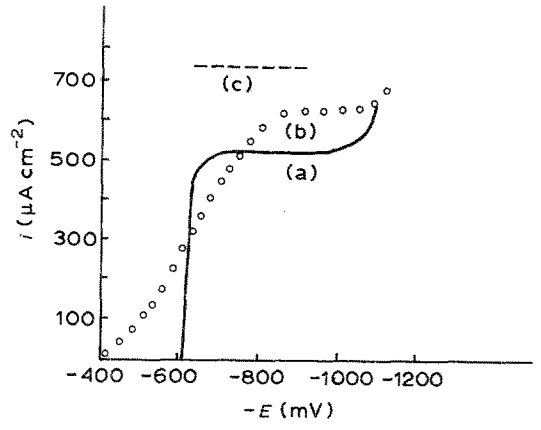

Fig. 8. Potentiostatic cathodic impedance characteristics of rotating carbon steel (XC38) electrode, respectively, in (a) 3% NaCl, (b) 3% NaCl + 10^{-2} M $C_{14}H_{26}N_2$. N = 1000 r.p.m. temperature = 30° C. The electrode was maintained for 30 min at E_{corr} before measurements. Theoretical current value according to Levich equation is represented by (c).

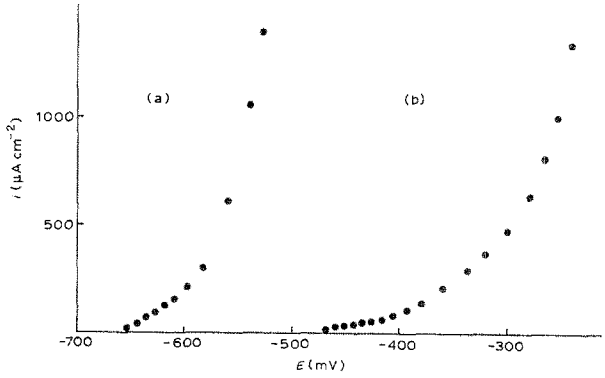

Fig. 9. Galvanostatic anodic characteristics of carbon steel (XC38) electrode in (a) 3% NaCl, (b) 3% NaCl + 10^{-2} M $C_{14}H_{26}N_2$. N = 1000 r.p.m.; temperature = 30° C. The electrode was maintained for 1 h at E_{corr} before measurements.

Table 2. R and C values estimated from electrochemical impedance measurements for a carbon steel electrode in 3% NaCl + 10^{-2} M $C_{14}H_{26}N_2$. Temperature = 30° C and N = 1000 r.p.m. The electrode was maintained for 1 h at e_{corr} before measurements were initiated

$i(\mu A\,cm^{-2})$	−300	−160	−100	−40	−20	0	+40	+80	+120	+200	+400	+1000
$R(\Omega cm^2)$	860 ± 30	940 ± 10	1040 ± 10	1450 ± 40	1950 ± 50	980 ± 40	840 ± 10	770 ± 20	610 ± 20	370 ± 10	170 ± 5	70 ± 3
$C(\mu F\,cm^{-2})$	4630 ± 200	1880 ± 50	860 ± 30	844 ± 50	392 ± 20	318 ± 25	333 ± 10	269 ± 20	238 ± 20	193 ± 3	165 ± 7	120 ± 6
Ri(mV)	258 ± 9	150.4 ± 3	104 ± 1	58 ± 2	39 ± 2	-	33.6 ± 1	61.6 ± 4	73.2 ± 4	74 ± 3	68 ± 4	70 ± 3

measurements (74 mV). This means that the inhibitor acts by modifying the anodic dissolution mechanism.

In the cathodic region, although the resistance decreases at low overvoltages, the Ri_c product was not constant (Table 2). This reflects the increasing influence of bulk transport and confirms the hypothesis of the existence of a cathodic region with mixed kinetics.

Calculation of the corrosion current density from the Stern and Geary relation [17], with parameters $R = 925 \pm 75\,\Omega cm^2$, $b_\alpha = 161 \pm 10$ mV gave the $i_{corr} = 42 \pm 10\,\mu A\,cm^{-2}$. This value is consistent with that resulting from the steady-state measurements.

The above results indicate that, for a concentration of 10^{-2} M, $C_{14}H_{26}N_2$ is clearly active in the anodic region. The oxygen reduction reaction is controlled by mixed kinetics in the vicinity of E_{corr} ($i_{corr} \ll i_L$) and by pure diffusion kinetics (diffusion plateau) at high cathodic overvoltages. This compound then acts by modification of the dissolution mechanism and not simply by a diminution of the active area of the electrode.

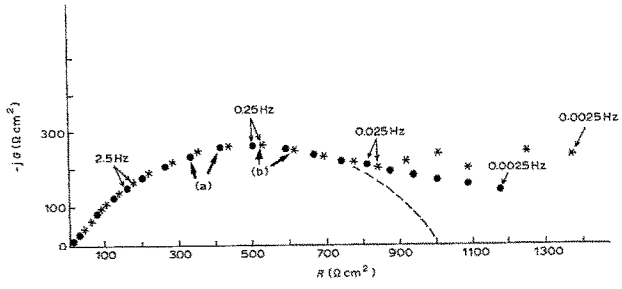

Fig. 10. Impedance diagrams in 3% NaCl + 10^{-2} M $C_{14}H_{26}N_2$ for two rotation speeds (N) at 30° C: (●) 200 and (*) 2000 r.p.m. The electrode was maintained for 30 min at E_{corr} before measurements.

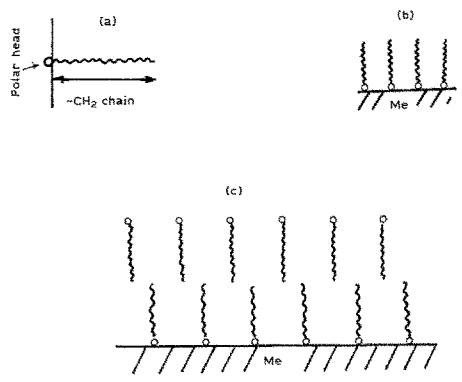

Fig. 11. Representation of (a) surfactant compound, (b) its adsorption at low concentration by polar head onto the metallic surface, and (c) the bilayer formation structure at high concentration on the interface metal-solution.

Values of i_{corr} found by different methods were in good agreement. The use of impedance diagrams did not show the existence of a capacitive loop at high frequencies as was also the case with $C_{10}H_{21}PO_3Na_2$. The inhibitor film formed on the surface acting as a barrier for oxygen diffusion is probably not very thick. All these observations tend to support this view, i.e., the establishment of an inhibitor double layer between the interface of the metal and the solution. The structure of this layer may involve a first adsorbed layer due to the polar head groups and a second stabilized layer resulting from the hydrophobic character of the $-CH_2$ groups chain (see Fig. 11). A general conclusion is given in Part II of this paper (following).

Acknowledgements

The authors are very indebted to Dr Max Costa, Directeur du Laboratoire d'Electrochimie du CNRS, and to Dr Robert Reeves for interesting and fruitful discussions. The technical help of Mrs Annie Plaza is also gratefully acknowledged.

References

[1] I. Epelboin, M. Keddam and H. Takenouti, Proc. 5th Int. Cong. Metall. Corr., Tokyo (1972) p. 90.
[2] R. D. Amstrong, M. F. Bell and A. A. Metcalfe, *J. Electroanal. Chem.* **77** (1977) 287.
[3] F. Dabosi, C. Deslouis, M. Duprat and M. Keddam, *J. Electrochem. Soc.* **130** (1983) 761.
[4] A. Bonnel, F. Dabosi, C. Deslouis, M. Duprat, M. Keddam and B. Tribollet, *J. Electrochem. Soc.* **130** (1983) 753.
[5] A. de Savignac and A. Lattes, *Werkstoffe and Corrosion*, **33** (1982) 203.
[6] Y. Derbali, M. Duprat, A. Lattes and A. de Savignac, *J. Soc. Chim. de Tunisie* **2** (1986) 35.
[7] G. Schmitt, Proc. 6th European Symposium on Corrosion Inhibitors, Ann. Univ. Ferrara, Sez. V, Sup. no. 8 (1985).
[8] Y. Derbali and A. Srhiri, *J. Soc. Chim. de Tunisie* **2** (6) (1987) 15.
[9] A. Ben-Bachir, F. Dabosi, Y. Derbali, M. Etman, A. Lattes and A. Srhiri, *J. Appl. Electrochem.* **21** (1991) 261–266.
[10] Y. Derbali, Thesis State, Toulouse, France (1985).
[11] A. Srhiri, Thesis State, Toulouse, France (1985).
[12] M. Duprat, N. Bui and F. Dabosi, *Corrosion* **35** (1979) 392.
[13] C. Gabrielli and M. Keddam, *Electrochim. Acta* **19** (1974) 355.
[14] V. G. Levich, 'Physicochem. Hydrodynamics', Prentice Hall, Englewood Cliffs, NJ (1962).
[15] F. Fabosi, C. Deslouis, M. Duprat, M. Keddam and B. Tribollet, *J. Electrochem. Soc.* **130** (1983) 753.
[16] M. Duprat, Thesis State, Toulouse, France (1981).
[17] F. M. Stern and A. L. Geary, *J. Electrochem. Soc.* **104** (1957) 56.
[18] W. Warburg, *Ann. Physik* **6** (1899) 125 and *Wied. Ann.* **67** (1899) 483.